applied sciences

MDPI

Article

Development of the Algorithmic Basis of the FCAZ Method for Earthquake-Prone Area Recognition

Sergey M. Agayan [1,*], Boris A. Dzeboev [1], Shamil R. Bogoutdinov [1,2], Ivan O. Belov [1], Boris V. Dzeranov [1] and Dmitriy A. Kamaev [3]

[1] Geophysical Center of the Russian Academy of Sciences, 119296 Moscow, Russia
[2] Schmidt Institute of Physics of the Earth of the Russian Academy of Sciences, 123995 Moscow, Russia
[3] Research and Production Association "Typhoon", 249038 Obninsk, Russia
* Correspondence: s.agayan@gcras.ru

Abstract: The present paper continues the series of publications by the authors devoted to solving the problem of recognition regions with potential high seismicity. It is aimed at the development of the mathematical apparatus and the algorithmic base of the FCAZ method, designed for effective recognition of earthquake-prone areas. A detailed description of both the mathematical algorithms included in the FCAZ in its original form and those developed in this paper is given. Using California as an example, it is shown that a significantly developed algorithmic FCAZ base makes it possible to increase the reliability and accuracy of FCAZ recognition. In particular, a number of small zones located at a fairly small distance from each other but having a close "internal" connection are being connected into single large, high-seismicity areas.

Keywords: FCAZ; DPS; earthquake-prone areas; density; finite metric spaces; connectivity; isolation

check for updates

Citation: Agayan, S.M.; Dzeboev, B.A.; Bogoutdinov, S.R.; Belov, I.O.; Dzeranov, B.V.; Kamaev, D.A. Development of the Algorithmic Basis of the FCAZ Method for Earthquake-Prone Area Recognition. *Appl. Sci.* **2023**, *13*, 2496. https://doi.org/10.3390/app13042496

Academic Editors: Shiyong Zhou and Ke Jia

Received: 8 November 2022
Revised: 9 February 2023
Accepted: 12 February 2023
Published: 15 February 2023

Copyright: © 2023 by the authors. Licensee MDPI, Basel, Switzerland. This article is an open access article distributed under the terms and conditions of the Creative Commons Attribution (CC BY) license (https://creativecommons.org/licenses/by/4.0/).

1. Introduction

The aim of seismic hazard assessment is to analyze and predict the parameters of seismic impact for future strong earthquakes. The first methods for finding solutions to this problem were deterministic (deterministic seismic hazard analysis (DSHA)) [1,2]. In DSHA, a seismic hazard is assessed for the maximum possible earthquake magnitude in each zone of seismic source occurrence over the shortest distance. A disadvantage of DSHA is that the timing (earthquake frequency and associated uncertainty) is often neglected. Only one scenario is used which describes the maximum possible earthquake [1–5].

In the 1970s, the development of probabilistic seismic hazard maps at the national, regional, and urban (microzonation) scales began [6–9]. In the 1990s, probabilistic methods began to prevail over deterministic ones. Currently, there are two main directions in research on seismic hazard assessment: probabilistic (probabilistic seismic hazard assessment (PSHA)) [10] and neodeterministic (neodeterministic seismic hazard assessment (NDSHA)) [11,12].

NDSHA allows a deterministic description of the seismic ground motion caused by an earthquake with a given epicentral or hypocentral distance and magnitude [13]. NDSHA methods are based on modeling in terms of detailed knowledge of the earthquake source [14–16] and the scenario of seismic wave propagation [17].

One of the key conditions for the successful application of NDSHA is the availability of adequate information about the areas prone to strong earthquakes in the studied region. The flexibility of NDSHA makes it possible to successfully incorporate additional information about areas prone to strong earthquakes obtained using independent methods and calculations. This reduces the existing gaps in knowledge about seismicity obtained from earthquake catalogs [18]. It was demonstrated in [19,20] that the use in NDSHA of additional knowledge about the areas prone to strong earthquakes, obtained by applying

pattern recognition methods [21–24], makes it possible to create effective preventive seismic hazard maps.

The fundamental possibility of using methods and algorithms of pattern recognition for earthquake-prone area recognition was first substantiated by the eminent mathematician I.M. Gelfand et al. in 1972 [25]. The formalized approach developed by them was subsequently called earthquake-prone areas (EPA) [21–23]. Over the past 50 years, since its inception, EPA has been used to recognize strong earthquake-prone areas in a number of mountainous countries in the world. A posteriori estimates of the recognition reliability that were obtained based on the analysis of the locations of the epicenters of strong earthquakes that occurred in the considered regions after receiving results for them became a confirmation of the effectiveness of using pattern recognition to identify territories with potentially high seismicity [24].

The authors of [21,26] described in detail the still-existing significant difficulties of applying EPA in practice. The latter served as the fundamental basis for the beginning of research at the Geophysical Center of the Russian Academy of Sciences, dedicated to the development of the ideological, system-mathematical, and computational base for earthquake-prone area recognition. As part of these studies, the algorithmic system of formalized clustering and zoning (FCAZ) [27,28] was developed, which is an unsupervised pattern recognition method. FCAZ is based on the classification of recognition objects by clustering. The epicenters of weak earthquakes are used as recognition objects.

Note that clustering is an important tool in the mining of geophysical data [29]. Clustering studies on earthquake epicenters [30–35] have been actively developed since the early 1990s [36]. As a rule, they are aimed at achieving two goals: revealing the characteristics of clusters and their relationship with the physical properties of the Earth's crust [37–40] and the declustering [29,31] of earthquake catalogs [41].

The analysis of earthquake epicenters with classical clustering algorithms is associated with difficulties [29,36]. It turns out that algorithms that take into account the "density" of the locations of objects are effective due to their ability to find clusters of an arbitrary shape even with significant data noise [29]. Within the framework of the scientific direction of discrete mathematical analysis (DMA) [42–44], created and developed at the Geophysical Center of the Russian Academy of Sciences, based on fuzzy mathematics and fuzzy logic under the general name DPS clustering, a complex of topological filtering algorithms is being developed that takes into account the density of the objects being classified [45–47]. It should be noted that DPS clustering algorithms are actively and effectively used in various geological and geophysical studies (analysis of earthquake catalogs, searching for signals on geophysical records, the problem of radioactive waste disposal, etc. [26,47–50]). DPS clustering is the algorithmic core of the FCAZ method [28].

FCAZ makes it possible to effectively recognize earthquake-prone areas (with a magnitude $M \geq M_0$) based on the clustering study of the catalog of seismic events [21]. In its original form, FCAZ was a sequential application of DPS clustering algorithms and the Ext algorithm [26]. The fundamental difference between FCAZ and its predecessors, particularly EPA, is the presence of a formalized block (algorithm) Ext. This implements the transition from the classification of point objects into high- and low-seismicity zones to the original flat high-seismicity zones. Ext formalizes the construction of a unique mapping of DPS clusters into flat zones of nonzero measure inside and on the boundary of which an earthquake with $M \geq M_0$ may occur [28]. FCAZ made it possible to move from simple pattern recognition to system analysis in the problem of earthquake-prone area recognition. In particular, with the help of FCAZ, it was possible to uniquely distinguish a subsystem of high-seismicity zones from a non-empty complement using an exact boundary.

Previously, FCAZ was used to successfully recognize earthquake-prone areas in the Andean mountain belt of South America, on the Pacific coast of the Kamchatka Peninsula and the Kuril Islands in California, in the Baikal-Transbaikal and Altai-Sayan regions, in the Caucasus, and in the Crimean Peninsula and northwestern Caucasus. A detailed

description of the FCAZ method, its mathematical apparatus, and the results obtained is given in [26].

It should be noted that at present, in parallel with the mathematical tools described here by the authors of earthquake-prone area recognition, methods for seismic hazard and subsequent seismic risk assessment are being created and developed based on other ideological foundations and mathematical solutions [2,51–57]. Most of them are still part of PSHA, although in recent years, there have been more and more publications in which PSHA has been criticized [2].

Returning to DPS clustering, it should be noted that, conceptually, its initial concept is a fuzzy model of the fundamental mathematical "limit" property. It is called the density and is a non-negative function that depends on an arbitrary subset and any point in the initial space in which clustering is assumed. The value of the density should be understood as the strength of the connection between a subset and a point, as the degree of influence of a subset on a point, or dually as the degree of limiting a point to a subset.

Nontrivial densities always exist in finite metric spaces (FMS). By fixing the density level α and interpreting it as a limit level, we can introduce the notion of discrete perfection with a level α. The set in the initial space is called discretely perfect with a level α (α-DPS set or just DPS set) if it consists of all points of the original space's α limit.

A rigorous theory of DPS sets (DPS theory) was constructed within the framework of DMA, in which, in particular, it is shown that DPS sets have the properties of clusters. The currently developed DPS clustering algorithms (DPS algorithms) operate in finite metric spaces and depend on a number of parameters, the main ones of which are the density P, its level α, and the local survey radius r, and they have three stages [43,46].

In the first stage, topological filtering of the original space is carried out, and its noise is cleared. DPS algorithms iteratively cut out from the original space the maximum α-perfect subset, the existence and uniqueness of which is guaranteed by the DPS theory.

In the second stage, the DPS algorithm splits the result of the first stage into r-connected components, which according to the DPS theory will be DPS sets. These are local DPS clusters. Due to the locality of the viewing radius, the division into r-connected components of the maximum α-perfect subset at the second stage is often small, detailed, and needs to be enlarged. This is the essence of the third and final stage of DPS clustering. Its result will be the representation of the maximum DPS subset in the form of a disjunct union of groups of local DPS clusters, each of which is a fragmentary manifestation (edge) of the global anomalous entity behind it in the original FMS. A detailed description of all DPS stages will be given below using the example of the SDPS algorithm, which is the most famous of the DPS algorithms.

This article is devoted to the further development of both DPS clustering and, in general, the mathematical apparatus of the FCAZ method. In the example of California, the advantages of strong earthquake-prone area recognition based on the developed algorithmic tools of the FCAZ method are shown.

2. Materials and Methods: SDPS Algorithm

Historically, the first in a series of DPS algorithms was the set theoretic SDPS algorithm [26,47,58]. It is based on the density S, which conveys the degree of concentration of the initial FMS X around each of its points x (the most natural understanding of the density X in x) (Figure 1). The result of SDPS is condensed groups in $X \leftrightarrow$ sets that locally contain "many X" and formally correspond best to empirical clusters.

Let us move on to a precise presentation of the SDPS algorithm.

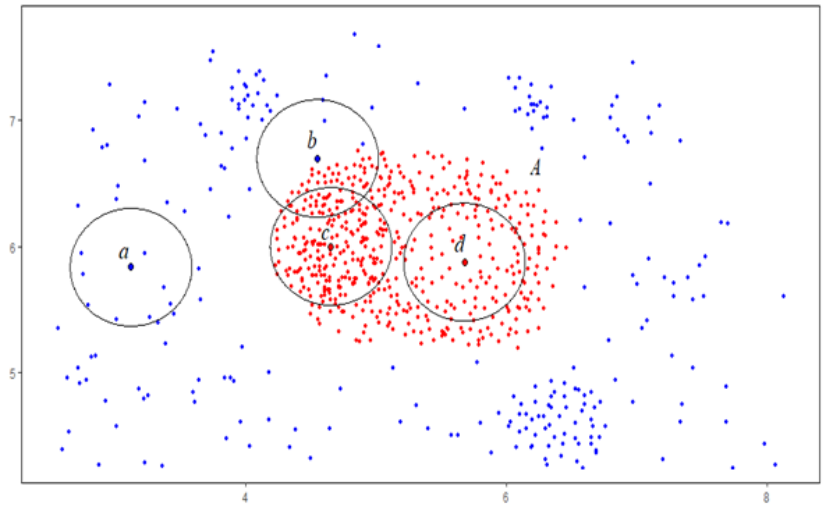


Figure 1. The concept of density relative to a set. Four points (a, b, c, and d) are selected in the initial array X. The density S in them relative to the subset A (red dots) is equal to the number of points from A that fall into the balls indicated in the figure. Point c will be densest with respect to A, followed by points b, d, and a.

2.1. Density S

Let X be a finite subset in the Euclidean plane Π with a distance d. The density S is a non-negative functional relationship between an arbitrary subset $A \subset X$ and any point $x \in X$: $S(A, x) \leftrightarrow S_A(x)$. Thus, the density $S_A(x)$ is also defined in the case where $x \notin A$.

S is determined by two parameters: the localization radius r and the center parameter $p \geq 0$, which takes into account the distance to x in the ball $D_A(x, r) = \{a \in A : d(x, a) \leq r\}$:

$$S_A(x) = S_A(x|r, p) = \sum_{y \in D_A(x,r)} \left(1 - \frac{d(x, y)}{r}\right)^p. \quad (1)$$

With $p = 0$, we obtain the usual number of points in $D_A(x, r)$:

$$S_A(x|r, 0) = |D_A(x, r)|.$$

2.2. First Stage

Set the level α of the density S, let $X^0(\alpha) = X$, and define the sequence of sets $X^{i+1}(\alpha) = \{x \in X^i(\alpha) : S_{X^i(\alpha)}(x) \geq \alpha\}, i = 0, 1, \ldots$. This does not increase $X^i(\alpha) \supseteq X^{i+1}(\alpha)$, and therefore, due to the finite nature of X, it will necessarily stabilize from some moment i^*:

$$X = X^0(\alpha) \supset X^i(\alpha) \supset \cdots \supset X^{i^*}(\alpha) = X^{i^*+1}(\alpha) = \cdots \leftrightarrow X(\alpha). \quad (2)$$

By replacing in the equality $X^{i^*+1}(\alpha) = \{x \in X^{i*}(\alpha) : P_{X^{i*}(\alpha)}(x) \geq \alpha\}$ the sets $X^{i*}(\alpha)$ and $Xi^* + 1(\alpha)$ on $X(\alpha)$, we obtain the equality

$$X(\alpha) = \{x \in X(\alpha) : P_{X(\alpha)}(x) \geq \alpha\},$$

which indicates the α density of the set $X(\alpha)$ in the space X even at its points. Such a set in X is called α discretely perfect:

Definition 1. *A subset A in X is α discretely perfect if*

$$A = \{x \in X : S_A(x) \geq \alpha\}. \quad (3)$$

The first stage (SDPS_1) of the SDPS algorithm is to build $X(\alpha)$ (i.e., transition from the entire set X to a subset $X(\alpha)$: $\mathrm{SDPS}_1 : X \to X(\alpha)$). The result ($X(\alpha)$) of the first stage of the SDPS algorithm will also be referred to as $\mathrm{SDPS}(X)$ or $\mathrm{SDPS}(\alpha, r, p)(X)$. The cutting process (Equation (2)) is shown in Figure 2, from which, in particular, it can be seen that the first stage of SDPS is a topological filtering of the space X (i.e., clearing it of noise).

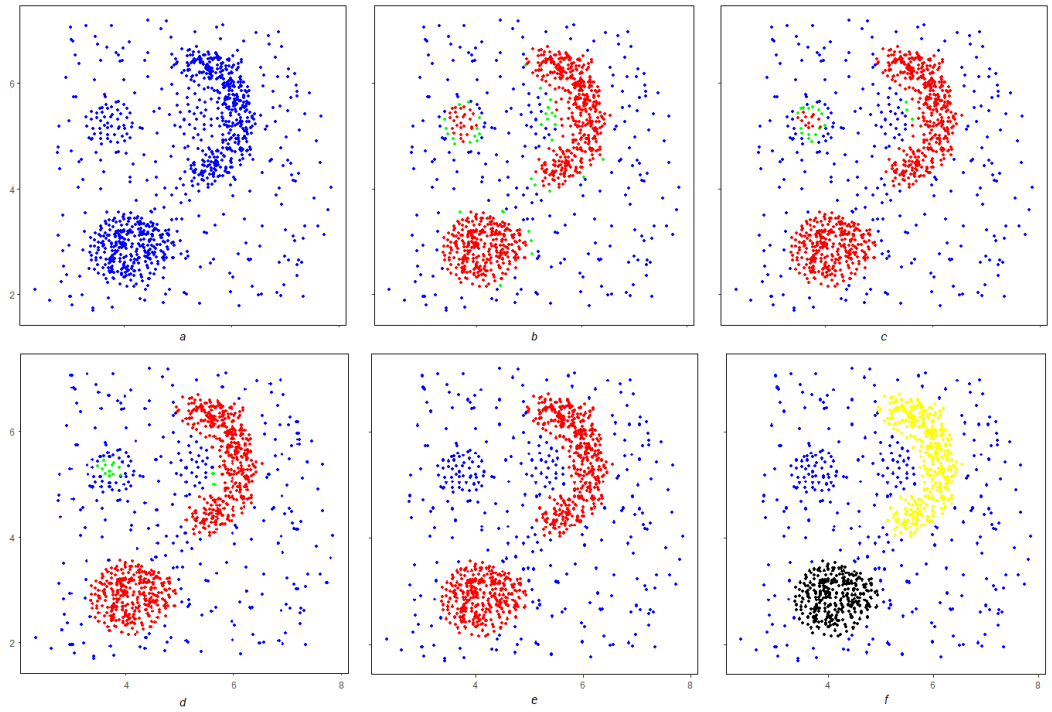


Figure 2. Application of the SDPS algorithm to the array X (**a**). Four iterations are shown in (**b**–**e**). The result is a local α-perfect subset of $X(\alpha)$ in X (**e**). The green points in figures (**b**–**d**) show the points that did not pass the next iteration in SDPS. SDPS further split $X(\alpha)$ into connected components (yellow and black subsets (**f**)).

The examples below illustrate the general nature of the dependence of the SDPS algorithm on the parameters at the first stage: the smaller the radius r, and the larger the parameters p and α, the more rigorous the SDPS was, and the denser and smaller its resulting $\mathrm{SDPS}_1(X)$ was:

Example 1. *The initial array X (Figure 3a) shows the inverse nature of the dependence of the SDPS algorithm on the density level α. By raising it, we went inside the condensations, finding dense nuclei already in them (Figure 3b,c)*

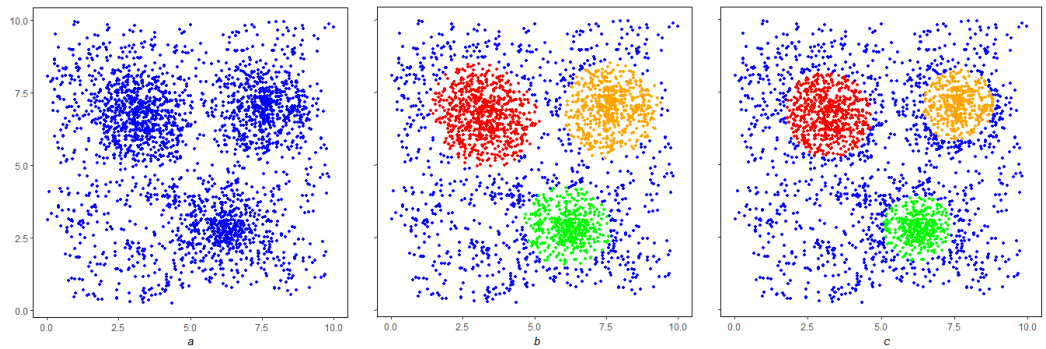


Figure 3. The inverse character of the dependence of the first stage of SDPS on the density level, where (**a**) is the initial array X and (**b**,**c**) have sets shown in red, yellow, and green for $\mathrm{SDPS}(\alpha, r, p)(X)$ and $\mathrm{SDPS}(\bar{\alpha}, r, p)(X)$ for $\alpha < \bar{\alpha}$.

Example 2. *Under the conditions of Example 1, the direct nature of the dependence of the SDPS algorithm on the vision radius r is shown. By lowering it by passing from r to $\bar{r} < r$, we made the SDPS algorithm more local with the aim of finding smaller condensations (Figure 4). All small condensations in Figure 4b are shown in black.*

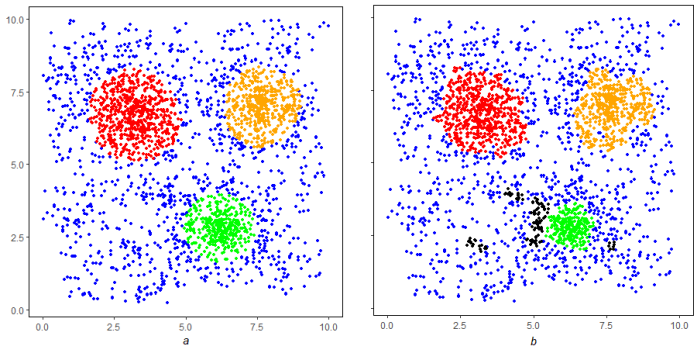


Figure 4. Direct dependence on the radius of localization of the first stage of SDPS when moving from SDPS$(\alpha, r, p)(X)$ (**a**) to SDPS$(\alpha, \bar{r}, p)(X)$ (**b**) with $r > \bar{r}$ on the array X (Figure 3a). Finer black condensations were added to the red, yellow and green ones.

Example 3. *In the conditions in Example 1, the inverse nature of the dependence of the SDPS algorithm on the parameter p was shown. By increasing it by going from p to $\bar{p} > p$, we made the SDPS algorithm more rigorous (Figure 5).*

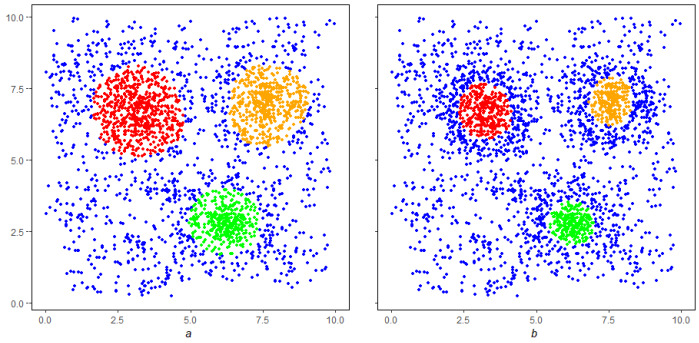


Figure 5. The inverse nature of the dependence of the first stage of SDPS on the center parameter. For $\bar{p} > p$, the result of SDPS$(\alpha, r, \bar{p})(X)$ (**b**) was more rigorous than the result of SDPS$(\alpha, r, p)(X)$ (**a**) on array X (Figure 3a).

2.3. Second Stage

Figure 6b shows the result of the first stage SDPS$_1(X)$ for the array X shown in Figure 6a. It is clear that it needed "reasonable" partitioning. In the SDPS algorithm, the second and third stages are devoted to this.

At the second stage, the set $X(\alpha)$ is partitioned into non-intersecting r-connected components (Figure 6c) which, of course, must be included in any reasonable partition of $X(\alpha)$. There are two reasons for this, and they are given below:

Definition 2. *Points x and y in $X(\alpha)$ are called r-connected if in $X(\alpha)$, there is a chain of r close-to-each-other points $x_0, \ldots, x_n$ with a start $x = x_0$, end $y = x_n$, and distances $d(x_i, x_{i+1}) \leq r, i = 0, \ldots, n-1$.*

The r connectivity relation is an equivalence that splits $X(\alpha)$ into disjunctive r connectivity components which, depending on the context, will be denoted below as c or c_k, $k = 1, \ldots, k^* = k^*(X(\alpha), r)$.

The second stage of the SDPS algorithm, which we will denote as $SDPS_2$, consists of constructing the c components. Their collection, as well as the partition $X(\alpha)$ associated with them, will be denoted identically as $C_r(X(\alpha))$, and thus

$$C_r(X(\alpha)) = \{c_k|_1^{k^*}\} \text{ and } C_r(X(\alpha)) \leftrightarrow X(\alpha) = \vee_{k=1}^{k^*} c_k. \quad (4)$$

This is the result of the second stage of the SDPS algorithm: $SDPS_2(X) = C_r(SDPS(X))$.

Rationale (first reason): r is the localization radius in the SDPS algorithm, and therefore any points that are r close to each other are considered close and must necessarily be included in the same partition component $X(\alpha)$ (the partition should not break close points).

Rationale (second reason): the components of the r connectivity are separated from each other by more than r, so the density S of each of them at any point from the other component is equal to zero. Hence, the conclusion is that each component of the r connection in $X(\alpha)$ is itself discretely perfect, since it independently provides the necessary level α of the density S at each of its points and is equal to zero at other points.

Figure 6 shows that the result of cutting (red dots in Figure 6b) was split in the second stage into 24 r-connected components, shown in Figure 6c with different colors.

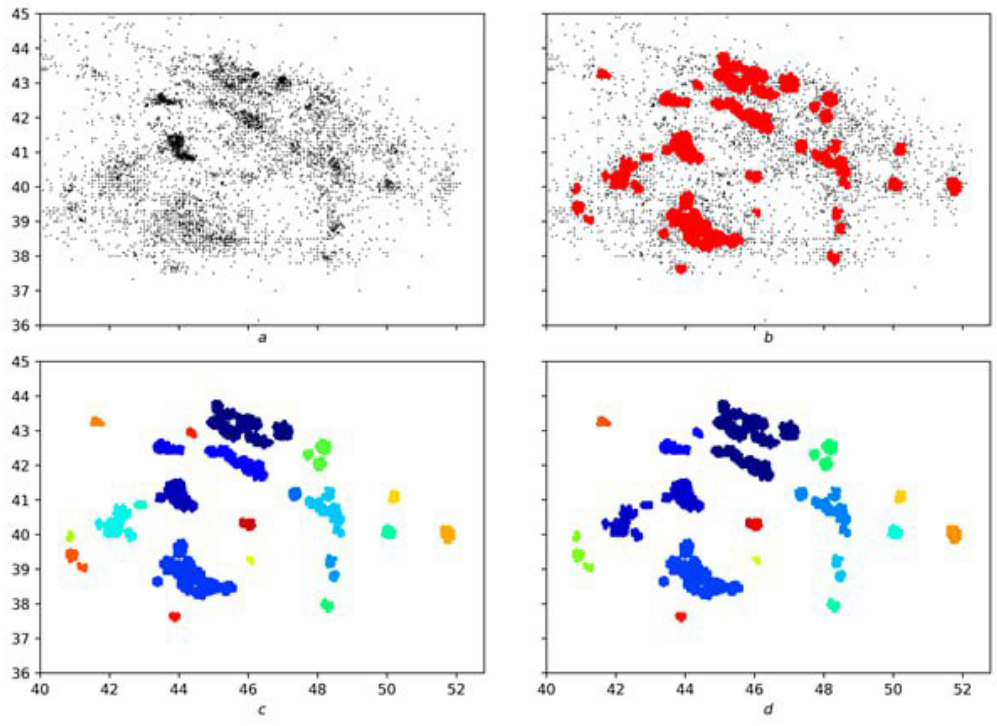


Figure 6. (**a**) Initial array X. (**b**) Result of the first stage of the SDPS algorithm. (**c**) Result of the second stage of the SDPS algorithm with r connectivity components (uniform in color sets). (**d**) Result of the third stage of the SDPS algorithm with edges and quasi-edges (uniform in color sets).

2.4. The Third Stage

The results of the second stage may be enough (Figures 3–5) or may not (Figure 6c). The expert E decides. He or she perceives the second stage $SDPS_2(X)$ as a given that is not subject to further internal transformation, considering each component of the r connectivity $c \in SDPS_2(X)$ to be a single and indivisible spot (big point).

The spots $c = cX(\alpha)$ are interpreted by the expert E as single exits (manifestations) of global anomalous entities in X. To understand their true scale, additional connection of spots, if possible, may be needed. This is the third and final stage of the SDPS algorithm.

The expert E considers a set of spots $C \subset SDPS_2(X)$ to be one whole if any two spots in it can be connected by a chain of close (in his or her opinion) intermediate transitions.

This gives the expert a reason to conclude that C is not random and that the set of spots (r components of connectivity) included in C is a collective but fragmentary manifestation (edge) of some global anomalous entity in X.

We denote with χ_E the partition of the spot space $\mathrm{SDPS}_2(X)$ into such "non-random" sets C_i:

$$\chi_E \leftrightarrow \mathrm{SDPS}_2(X) = \vee_{i=1}^{i^*(E)} C_i, C_i = \left\{ C_{ij} |_{j=1}^{j^*(i)} \right\}. \quad (5)$$

This is the third stage of the SDPS algorithm ($\mathrm{SDPS}_3(X) = \chi_E$), and it depends on the expert E's analysis of the initial space X and the first and second SDPS stages of it:

$$\chi_E = \chi_E(X, \mathrm{SDPS}_1(X), \mathrm{SDPS}_2(X)). \quad (6)$$

With such an analysis, for each set C_i, the question of proximity within it is generally solved individually.

In this paper, the simplest Boolean version of the third stage is presented where, based on the analysis of the space X only, the expert E develops its proximity threshold r_E, which is weaker than r ($r < r_E$) and splits the spot space $\mathrm{SDPS}_2(X)$ into r_E connectivity components ($\chi_E = C_{r_E} X(\alpha)$).

The parameters r and r_E are constructed using power law averaging of non-trivial distances in X:

$$r = \left(\frac{\sum_{x \neq y \in X} d(x,y)^{q(r)}}{|X|(|X|-1)} \right)^{1/q(r)},$$
$$r_E = \left(\frac{\sum_{x \neq y \in X} d(x,y)^{q(E)}}{|X|(|X|-1)} \right)^{1/q(E)}.$$

For the parameter r, numerous tests of the SDPS algorithm have established that the choice of $q(r) \in [-3, -2]$ can be considered optimal. The studies carried out in the framework of this work show that $q(E) \in [-2.5, -1.5]$. The intersection of the areas of parameters r and r_E is explained both by the fuzzy perception of proximity by the expert and by the diversity in construction of X.

Figure 6c shows the 24 r connectivity components (spots) obtained in the second stage, which combined into 15 r_E connectivity components (Figure 6d). Note that, in this case, $q(r) = -3.0$, and $q(r_E) = -2.3$.

2.5. SDPS and DBSCAN Algorithms

The cutting process (Equation (2)) was also valid for other density constructions, particularly for the derivative of S of the construction $\tilde{S}$: $\tilde{S}_A(x) = \max S_A(\tilde{x}), \tilde{x} \in D_A(x, r)$. The related S̃DPS algorithm was less rigorous than the SDPS algorithm. For the same parameters r, p, and α, $\mathrm{SDPS}(X) \subseteq \tilde{\mathrm{SDPS}}(X))$ always held and coincided with the well-known DBSCAN algorithm.

Figure 7b,c shows the results of the second stage of the SDPS and S̃DPS = DBSCAN algorithms, and Figure 7a shows traditional k-means clustering. All this gives grounds for the following conclusion: the SDPS algorithm in its first two stages, as in the well-known algorithms DBSCAN, OPTICS, and RSC [59,60], represents a new stage in cluster analysis, where modern cluster analysis algorithms first filter the initial space, clearing it of noise (first stage), and then the result is divided into homogeneous parts (second stage).

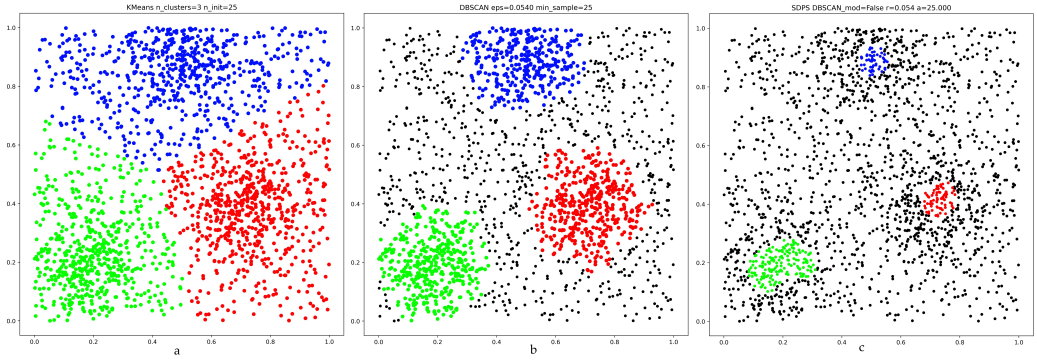


Figure 7. Comparison of the results of the algorithms. (**a**) Results of clustering with the k-means algorithm. (**b**) SDPS algorithm. (**c**) DBSCAN algorithm.

3. Immersion of a Finite Set into a Domain of Euclidean Space under DMA Methods

The results for the operation of the SDPS algorithm in its pure form were of little use for practical conclusions. Therefore, discrete expansions needed to be immersed in Euclidean domains, finding a compromise between the economy (scanability) and connectivity (smoothness) of such immersion. The resulting disjunctive regions would be areas of increased interest for the reasons that prompted the operation of the SDPS algorithm.

DMA methods help to solve the problem of immersing a finite set into the domain of a Euclidean space in the two-dimensional case. The solution is the result of the joint work of the Ext and Int algorithms. Ext was developed earlier, and it is responsible for the ability to scan the embedding. It is a component of FCAZ [26,50]. Int is responsible for the connectivity of the embedding. It is presented here for the first time and is the main theoretical result of this paper.

The initial data were a domain B in the Euclidean plane Ξ and a finite set A in B. The task was to construct a Euclidean shell $H(A)$ for A in B that satisfied the ability to scan and connectivity requirements formulated above.

3.1. Ext and Int Algorithms

Let us choose an orthonormal coordinate system xOy in Ξ so that $\Xi = \mathbb{R}^2(x, y)$ and also a regular pixel cover Π of the plane Ξ, consistent with the xOy coordinates.

The shell $\mathrm{Ext}(A)$ for A in B is obtained as the union of all pixels π from Π that intersect B and are close to A:

$$\mathrm{Ext}(a) = \cup\{\pi \in \Pi : ((\pi \cap B) \neq \varnothing) \wedge (\pi \text{ close to } A)\}. \quad (7)$$

Thus, it is necessary to determine the proximity π to A. There are several ways to accomplish this in DMA, namely quantiles, fuzzy comparisons, and Kolmogorov averages. Let us present the last option.

Let $c(\pi)$ denote the center of the pixel π, and define the distance $\rho(A, \pi)$ from A to π as the Kolmogorov averaging M_ν of the nontrivial distances between elements A and $c(\pi)$ with a negative index ν:

$$\rho(A, \pi) = M_\nu\{\rho(a, c(\pi)) : a \in A \wedge \rho(a, c(\pi)) \neq 0\},\ \nu < 0.$$

The proximity threshold $\rho(A|B)$ to A in B is also obtained using Kolmogorov averaging in the general case with another negative index ω:

$$\rho(A|B) = M_\omega\{\rho(A, \pi) : \pi \cap B \neq \varnothing\},\ \omega < 0.$$

The shell $\mathrm{Ext}(A)$ is formed by all pixels close to A in B:

$$\mathrm{Ext}(A) = \cup\{\pi : \rho(A, \pi) \leq \rho(A|B)\}.$$

Next, we turn to the Int. Let us fix any point b from B and, for any a from A other than b, denote with $\Theta_b(a)$ the angle in $[0, 2\pi)$ corresponding to the direction of $e_b(a)$ from b to a:

$$e_b(a) = \frac{b-a}{||b-a||} = (\cos\Theta_b(a), \sin\Theta_b(a)).$$

Let us properly order the set of angles $\Theta_b(A) = \{\Theta_b(a), a \in A \setminus b\}$ in $[0, 2\pi)$:

$$\Theta_b(A) \to \{\Theta_1 < \Theta_2 < \cdots < \Theta_n\},\ n = n(b, A)$$

and assume $\Theta_{n+1} = \Theta_1$.

The extended set $\overline{\Theta_b(A)} = \{\Theta_i|_1^{n+1}\}$ is responsible for the environment of the point b by the set A and helps to express it formally. If, for the chosen environment threshold $\Theta \in [0, \pi]$, all successive differences $\Theta_{i+1} - \Theta_i$ are less than Θ $(i = 1, \ldots, n)$, then the point b is considered to be environed by the set A (internal for A). Otherwise, the point b is considered external to A:

$$b \leftrightarrow \begin{matrix}\text{internal}\\ \text{external}\end{matrix} \text{ for } A, \text{ if } \max\{\Theta_{i+1} - \Theta_i|_1^n\} \begin{matrix}<\\ \geq\end{matrix} \Theta. \tag{8}$$

The connection (Equation (8)) with the locality threshold R makes the environing criterion more flexible by making it local, where b is locally internal (external) for A if b is internal (external) for the ball $D_A(b, R)$ according to Equation (8).

The shell $\mathrm{Int}(A)$ is formed by all pixels whose centers are internal to A:

$$\mathrm{Int}(A) = \{\pi \in \Pi : c(\pi) \text{ locally internal } A\}.$$

The shell $H(A)$ for A in B with the ability to scan and connectivity conditions is obtained by the union of $\mathrm{Ext}(A)$ and $\mathrm{Int}(A)$:

$$H(A) = (\mathrm{Ext} + \mathrm{Int})(A) = \mathrm{Ext}(A) \cup \mathrm{Int}(A).$$

Its construction depends on four parameters: two negative indices ν, ω for Ext, and the environing and locality thresholds Θ and R for Int.

Figure 8 shows the set A for which Figure 9 presents all the stages of constructing the shell H(A). The final result is shown in two ways: $H(A) = \mathrm{Ext}(A) \cup (\mathrm{Int}(A) \setminus \mathrm{Ext}(A))$ (Int against the background of Ext (Figure 9c)) and $H(A) = \mathrm{Int}(A) \cup (\mathrm{Ext}(A) \setminus \mathrm{Int}(A))$ (Ext against the background of Int (Figure 9d)).

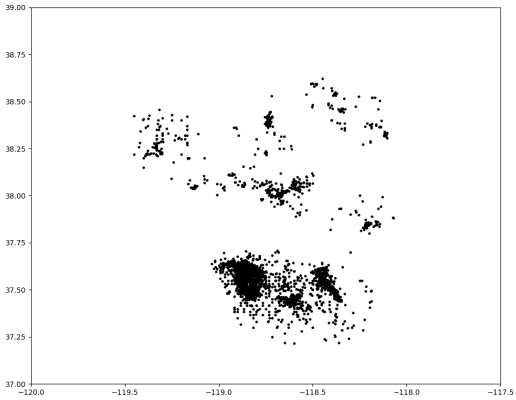


Figure 8. Initial array X for constructing the shell $H(A)$.

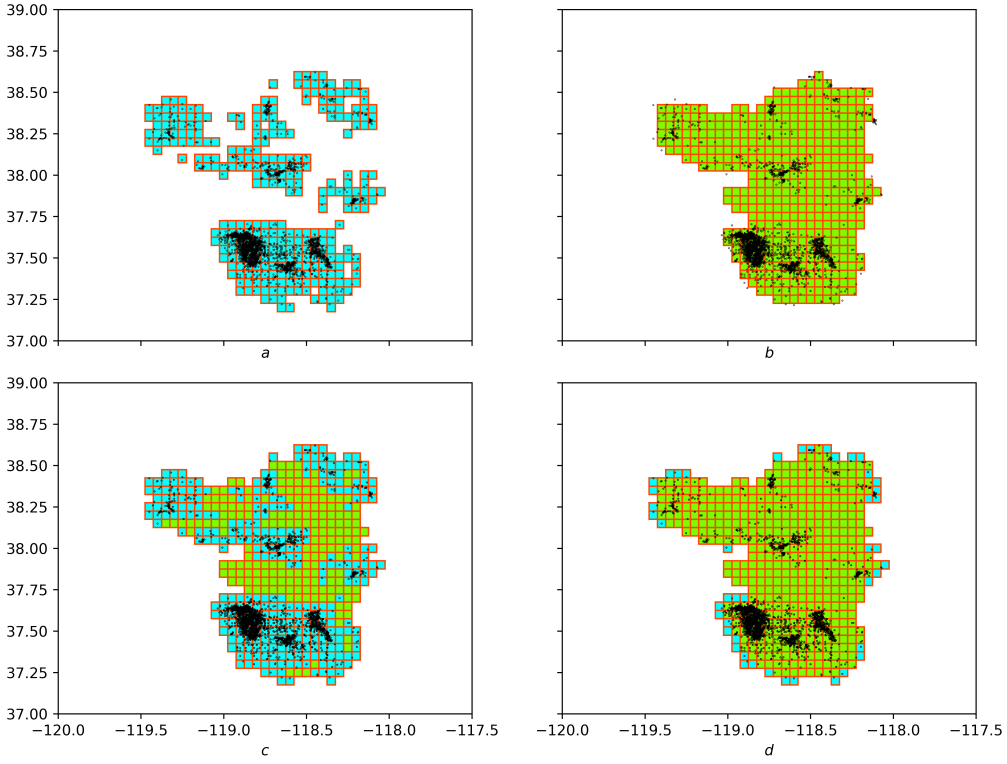


Figure 9. (**a**) Ext shell for the set A. (**b**) Shell of Int for the set A. (**c**) Shell $H(A) = \text{Ext}(A) \cup (\text{Int}(A) \setminus \text{Ext}(A))$ (Int against the background of Ext). (**d**) Shell $H(A) = \text{Int}(A) \cup (\text{Ext}(A) \setminus \text{Int}(A))$ (Ext against the background of Int).

3.2. FCAZ Method

FCAZ in its original version was a sequential combination of only the first stage of the SDPS algorithm and the Ext algorithm [28]:

$$\text{FCAZ}(X) = \text{Ext}(\text{SDPS}(X)).$$

The additional stages in the SDPS algorithm presented in this article, as well as Int algorithm, allowed us to continue the development of FCAZ. We propose a new variant of FCAZ associated with the Boolean version of SDPS, namely the joint use of Ext and Int algorithms, resulting in the SDPS algorithm on X in the form of decomposition:

$$\text{FCAZ}(X) = (\text{Ext} + \text{Int})(\text{SDPS}(X)).$$

Figure 10 shows an example of constructing FCAZ zones based on a developed mathematical apparatus.

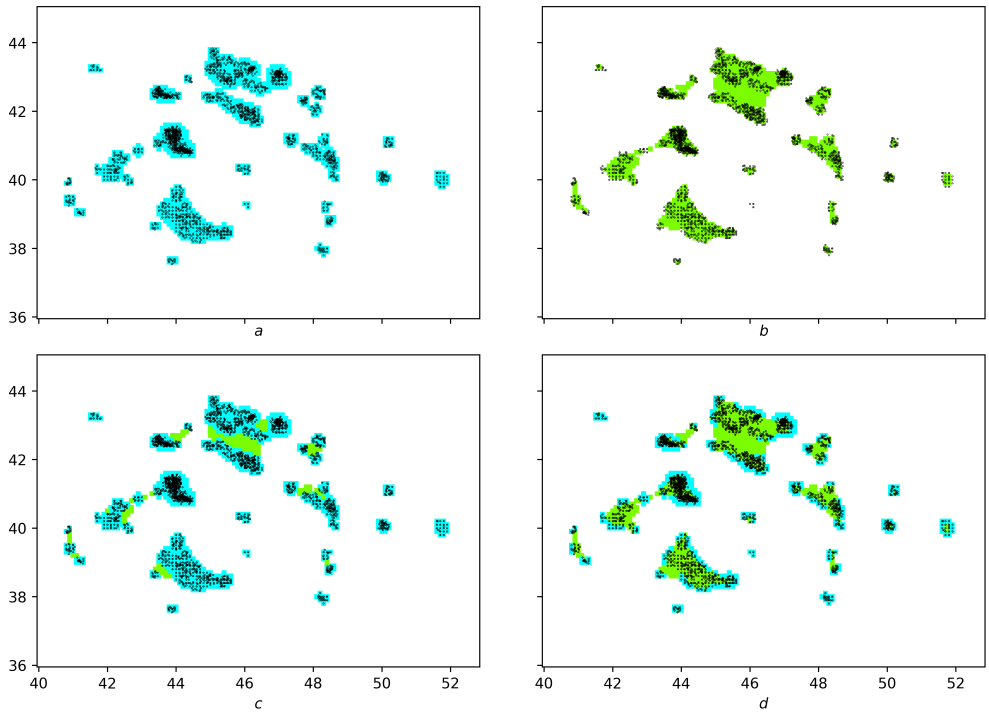


Figure 10. FCAZ zones constructed for the results from running the first stage of the SDPS algorithm on the array X (Figure 6b). (**a**) Extzones. (**b**) Int zones. (**c**) Int against the background of Ext. (**d**) Ext on the background of Int.

4. Discussion

As mentioned above, the FCAZ method in its initial form, which has been used to date to recognize the areas prone to the strongest, strong, and significant earthquakes in a number of mountainous countries of the world [26], is a sequential application of the first stage of the SDPS algorithm (in the papers devoted to FCAZ recognition, it is just the DPS algorithm) and the Ext algorithm, where $\mathrm{FCAZ}(X) = \mathrm{Ext}(\mathrm{DPS}(X))$ [28]. In the present work, the algorithmic base of the FCAZ method was substantially developed. Thus, in particular, its algorithmic base was expanded.

Using California as an example, let us consider the contribution of the Int algorithm developed in this paper to the mapping of potential high-seismicity zones (i.e., contouring of the recognized DPS clusters of epicenters of weak earthquakes). In Figure 11, the green and red colors show the results of FCAZ recognition of strong earthquake-prone areas with magnitudes $M \geq 6.5$ in California from [26]. Earthquake epicenters from the ANSS catalog (http://www.ncedc.org/anss/catalog-search.html, accessed on 1 January 2020) with $M \geq 3.0$ that occurred over the period of 1960–2012 were used as recognition objects (DPS clustering). The choice of the magnitude threshold $M = 3.0$ was carried out based on theoretical and practical analysis of the magnitude–frequency graphs for the entire considered region. The green color in Figure 11 shows the DPS clusters, while red shows the high-seismicity zones mapped by the Ext algorithm based on the clusters within which earthquakes with $M \geq 6.5$ can occur. In [26], the arguments in favor of the reliability of the performed recognition are presented in detail. In turn, it was shown in [50] that the result of FCAZ recognition in California depended little on the presence or absence of foreshock and aftershock sequences in the earthquake catalog, which is the source of recognition objects.

The black stars in Figure 11 show the epicenters of 33 earthquakes with $M \geq 6.5$ that occurred over the period of 1836–2010. The blue and white stars show the epicenters of events with $M \geq 6.5$ that occurred in 2014 and 2019 (i.e., after the end of the instrumental catalog, which made up a set of recognition objects). These events formed the material of a pure experiment. Thus, the consistency of the recognized FCAZ zones with the locations

of the epicenters of strong earthquakes that occurred more than 180 years ago, including the ones before and after the beginning of the instrumental catalog used in recognition, was checked.

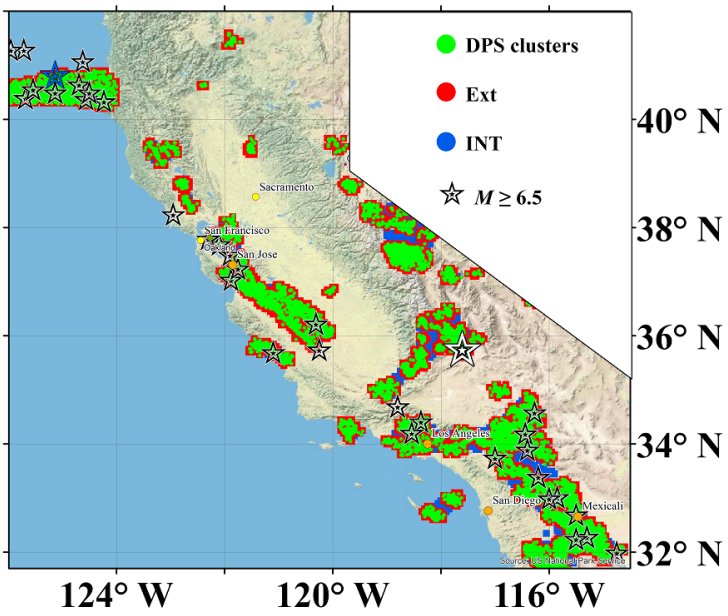


Figure 11. New FCAZ zones prone to earthquakes with $M \geq 6.5$ in California and earthquake epicenters with $M \geq 6.5$.

Out of 35 events with $M \geq 6.5$, only 5 (14.3%) epicenters did not fall into the recognized FCAZ-zones (Figure 11). At the same time, it should be noted that three epicenters located in the northwest of the region are located in the Pacific Ocean at a fairly large distance from the coast. Additionally, two epicenters of historical earthquakes did not fall into the FCAZ zones: near Fort Tehon (1857) and in San Francisco (1906). These earthquakes occurred long before the start of systematic instrumental observations of seismicity in California. Thus, for various reasons, there were not enough objects (earthquake epicenters with $M \geq 3.0$) to recognize the areas of these five strong earthquakes.

The positive result of the pure experiment should be noted: both epicenters fell strictly inside the FCAZ zones (Figure 11). At the same time, we emphasize that the epicenter of the earthquake on 6 July 2019 with $M = 7.1$ (white star in Figure 11) [61], being inside the FCAZ zones, was located outside the areas determined for the magnitude threshold $M = 6.5$ being high seismicity under the EPA method [21]. The latter once again emphasizes the modernity and reliability of the obtained FCAZ results.

The result of applying the new computational component Int in the FCAZ structure is shown in Figure 11 in blue against the background of red zones mapped by the Ext algorithm. Thus, we have a new shell $\mathrm{Ext(DPS)} \cup (\mathrm{Int(DPS)} \setminus \mathrm{Ext(DPS)})$ of high-seismicity DPS clusters in California, which we will consider in this paper as new FCAZ zones prone to strong earthquakes.

The new FCAZ zones had the same number of "miss target" errors. As before, five earthquake epicenters were outside the recognized zones. However, it should be noted that the development of the FCAZ algorithmic basis, including the expansion of the algorithmic base of the method, could not directly lead to a decrease in the number of target misses. The contribution of the updated mathematical toolkit of the method which significantly develops FCAZ-seismic zoning is as follows. At the second (described in detail above) stage of the application of the DPS algorithm in California, clusters were formed that were r-connected components (Equation (4)). According to the mathematical construction embedded in the third DPS stage, some of these connected components need to be combined into large clusters that have a close internal connection against the background of all

recognized dense condensations. However, the Ext algorithm does not always allow building a single FCAZ zone for clusters that are united at the third DPS stage. The Int algorithm effectively solves this problem.

From Figure 11, it can be seen that the result of the operation of the Int algorithm made it possible to combine several zones mapped by the Ext algorithm into individual high-seismicity areas. This was especially well observed in the south and east of the Sierra Nevada mountains, in the ocean area south of Los Angeles, as well as northeast of the city of San Diego. In the last location, Int made it possible to connect the edges of a large FCAZ zone mapped by the Ext algorithm. Thereby, the degree of falling into this zone of two strong earthquake epicenters increased. Before the application of the Int algorithm, these epicenters were located on the very edge of the recognized FCAZ zones.

From Figure 11, it can be concluded that the FCAZ recognition result obtained in California using the updated algorithmic base, which presented more interconnected potential high-seismicity zones, has a greater degree of reliability. Thus, based on the developed mathematical apparatus, the reliability and accuracy of the FCAZ recognition of areas prone to earthquakes were significantly increased. This in turn contributes to the prediction of damage from earthquakes and, for the first time, can be directly used to update seismic zoning maps.

5. Conclusions

Discrete mathematical analysis is a discrete data analysis method that uses scenarios of classical continuous mathematics, in which the fundamentals are replaced by fuzzy models of their discrete analogs. From a practical point of view, DMA is a new approach to data analysis focused on an expert and occupying an intermediate position between rigorous mathematical methods and soft combinatorial ones.

The solution to the problem within the DMA framework consists of two parts. The first one is informal, as it analyzes the logic of the expert, introduces the necessary concepts, and explains the scenarios and principles of the solution. The second has a formal characteristic. With the help of the DMA apparatus, all concepts receive rigorous definitions within the framework of fuzzy mathematics and fuzzy logic, and the schemes and principles become algorithms.

This article provides three such solutions:

- The SDPS algorithm is a DMA response to the empirical definition of a cluster as a connected set, the measure of the presence of which at each of its points is higher than at any other.
  The answer is a rigorous DPS set theory and DPS clustering based on it.
- The Ext algorithm is a DMA formalization of the scanning ability and proximity based on an empirical understanding with the help of Kolmogorov means (one of the main technical means of DMA).
- The Int algorithm is a DMA formalization of smoothness (insideness) based on the empirical logic of the circle with the help of Kolmogorov means and standard linear algebra.

It should be noted that DMA has all the necessary tools to generate unsupervised topological filtering and classification algorithms. Based on fuzzy sets and fuzzy logic, DMA can convey expert ideas about the spatial distributions of objects. DMA makes it possible to implement a system approach to the analysis of geophysical data in the problem of adequate seismic hazard assessment studied in the article.

In conclusion, we emphasize that based on the mathematical apparatus of the FCAZ method, which has been substantially developed based on DMA, in this work, new zones prone to earthquakes with $M \geq 6.5$ in California were constructed. A distinctive feature of the new FCAZ recognition system is the combination of a number of smaller zones located at a relatively small distance from each other into large, single, connected potential high-seismicity zones. Note that after applying the Int algorithm, the area of the FCAZ zones increased by only 6%.

The results presented in the present and previous works indicate the high reliability of the interpretation of FCAZ zones as earthquake-prone areas. The FCAZ method makes it possible to effectively recognize possible locations of future earthquakes solely from seismological data. We also note that the results of the FCAZ studies indicate that weak seismicity can actually "manifest" the properties of geophysical fields, which are used directly in the form of characteristics of recognition objects in other (similar to FCAZ) methodologies.

Author Contributions: All authors contributed to the study's conception and design. Conceptualization and original draft preparation, S.M.A., B.A.D. and S.R.B.; conceptualization, methodology, review and editing and validation, D.A.K. and B.V.D.; material preparation, formal analysis, data curation, and algorithm development, S.R.B. and I.O.B. All authors have read and agreed to the published version of the manuscript.

Funding: This work was conducted in the framework of budgetary funding of the Geophysical Center of RAS, adopted by the Ministry of Science and Higher Education of the Russian Federation.

Institutional Review Board Statement: Not applicable.

Informed Consent Statement: Informed consent was obtained from all subjects involved in the study.

Data Availability Statement: Not applicable.

Conflicts of Interest: The authors declare no conflict of interest.

Abbreviations

The following abbreviations are used in this manuscript:

DSHA	Deterministic seismic hazard analysis
PSHA	Probabilistic seismic hazard assessment
NDSHA	Neodeterministic seismic hazard assessment
EPA	Earthquake-prone areas
FCAZ	Formalized clustering and zoning
DMA	Discrete mathematical analysis
DPS	Discrete perfect sets
FMS	Finite metric space
SDPS	Sets discrete perfect sets

References

1. Mualchin, L. History of Modern Earthquake Hazard Mapping and Assessment in California Using a Deterministic or Scenario Approach. *Pure Appl. Geophys.* **2010**, *168*, 383–407. [CrossRef]
2. Wang, Z. Seismic Hazard Assessment: Issues and Alternatives. *Pure Appl. Geophys.* **2010**, *168*, 11–25. [CrossRef]
3. Atkinson, G.M. The Integration of Emerging Trends in Engineering Seismology. In Proceedings of the 13th World Conference on Earthquake Engineering, Lisbon, Portugal, 24–28 September 2012.
4. Kijko, A. Seismic Hazard. In *Encyclopedia of Solid Earth Geophysics*; Springer: Dordrecht, The Netherlands, 2011; pp. 1107–1121. [CrossRef]
5. Krinitzsky, E.L. How to combine deterministic and probabilistic methods for assessing earthquake hazards. *Eng. Geol.* **2003**, *70*, 157–163. [CrossRef]
6. Bommer, J.J.; Abrahamson, N.A. Why Do Modern Probabilistic Seismic-Hazard Analyses Often Lead to Increased Hazard Estimates? *Bull. Seismol. Soc. Am.* **2006**, *96*, 1967–1977. [CrossRef]
7. Ulomov, V.I. Seismic hazard of Northern Eurasia. *Ann. Geophys.* **1999**, *42*, 1023–1038. [CrossRef]
8. Zaalishvili, V.B.; Dzeranov, B.V.; Gabaraev, A.F. Seismic hazard assessment of the territory and construction of probability maps. *Geol. Geophys. Russ. South* **2011**, *1*, 48–58. (In Russian)
9. Shibaev, S.V.; Kozmin, B.M.; Imaev, V.S.; Imaeva, L.P.; Petrov, A.F.; Starkova, N.N. The February 14, 2013 Ilin-Tas (Abyi) earthquake (Mw=6.7), Northeast Yakutia. *Ross. Seismol. Zhurnal Russ. J. Seismol.* **2020**, *2*, 92–102. [CrossRef]
10. Cornell, C.A. Engineering seismic risk analysis. *Bull. Seismol. Soc. Am.* **1968**, *58*, 1583–1606. [CrossRef]
11. Panza, G.F.; Bela, J. NDSHA: A new paradigm for reliable seismic hazard assessment. *Eng. Geol.* **2020**, *275*, 105403. [CrossRef]
12. Panza, G.F.; Mura, C.L.; Peresan, A.; Romanelli, F.; Vaccari, F. Seismic Hazard Scenarios as Preventive Tools for a Disaster Resilient Society. In *Advances in Geophysics*; Elsevier: Amsterdam, The Netherlands, 2012; pp. 93–165. [CrossRef]
13. Skorkina, A.A. Scaling of two corner frequencies of source spectra for earthquakes of the Bering fault. *Russ. J. Earth Sci.* **2020**, *20*, 1–9. [CrossRef]

14. Dziewonski, A.M.; Chou, T.A.; Woodhouse, J.H. Determination of earthquake source parameters from waveform data for studies of global and regional seismicity. *J. Geophys. Res. Solid Earth* **1981**, *86*, 2825–2852. [CrossRef]
15. Mäntyniemi, P.; Tatevossian, R.E.; Tatevossian, T.N. Uncertain historical earthquakes and seismic hazard: Theoretical and practical considerations. *Geomat. Nat. Hazards Risk* **2013**, *5*, 1–6. [CrossRef]
16. Rebetsky, Y.L.; Tatevossian, R. Rupture propagation in strong earthquake sources and tectonic stress field. *Bull. De La Société Géologique De Fr.* **2013**, *184*, 335–346. [CrossRef]
17. Parvez, I.A.; Rosset, P. The Role of Microzonation in Estimating Earthquake Risk. In *Earthquake Hazard, Risk and Disasters*; Elsevier: Amsterdam, The Netherlands, 2014; pp. 273–308. [CrossRef]
18. Karapetyan, J.K.; Gasparyan, A.S.; Shakhparonyan, S.R.; Karapetyan, R.K. Registration and spectral analysis of waveforms of 10.24.2019 earthquake in the Caucasus using the new IGES-006 seismic sensor. *Russ. J. Earth Sci.* **2020**, *20*, 1–8. [CrossRef]
19. Peresan, A. The Contribution of Pattern Recognition of Seismic and Morphostructural Data to Seismic Hazard Assessment. *arXiv* **2015**, arXiv:1406.2932. [CrossRef]
20. Rugarli, P.; Vaccari, F.; Panza, G. Seismogenic nodes as a viable alternative to seismogenic zones and observed seismicity for the definition of seismic hazard at regional scale. *Vietnam. J. Earth Sci.* **2019**, *41*, 289–304. [CrossRef]
21. Gvishiani, A.D.; Soloviev, A.A.; Dzeboev, B.A. Problem of Recognition of Strong-Earthquake-Prone Areas: A State-of-the-Art Review. *Izv. Phys. Solid Earth* **2020**, *56*, 1–23. [CrossRef]
22. Gorshkov, A.I.; Soloviev, A.A. Recognition of earthquake-prone areas in the Altai-Sayan-Baikal region based on the morphostructural zoning. *Russ. J. Earth Sci.* **2021**, *21*, 1–16. [CrossRef]
23. Kossobokov, V.G.; Soloviev, A.A. Pattern recognition in problems of seismic hazard assessment. *Chebyshevskii Sb.* **2018**, *19*, 55–90. [CrossRef]
24. Soloviev, A.A.; Gvishiani, A.D.; Gorshkov, A.I.; Dobrovolsky, M.N.; Novikova, O.V. Recognition of earthquake-prone areas: Methodology and analysis of the results. *Izv. Phys. Solid Earth* **2014**, *50*, 151–168. [CrossRef]
25. Gelfand, I.M.; Guberman, S.I.; Izvekova, M.L.; Keilis-Borok, V.I.; Ranzman, E.J. Criteria of high seismicity, determined by pattern recognition. *Tectonophysics* **1972**, *13*, 415–422. [CrossRef]
26. Dzeboev, B.A.; Gvishiani, A.D.; Agayan, S.M.; Belov, I.O.; Karapetyan, J.K.; Dzeranov, B.V.; Barykina, Y.V. System-Analytical Method of Earthquake-Prone Areas Recognition. *Appl. Sci.* **2021**, *11*, 7972. [CrossRef]
27. Gvishiani, A.D.; Dzeboev, B.A.; Agayan, S.M. A new approach to recognition of the strong earthquake-prone areas in the Caucasus. *Izv. Phys. Solid Earth* **2013**, *49*, 747–766. [CrossRef]
28. Gvishiani, A.D.; Dzeboev, B.A.; Agayan, S.M. FCaZm intelligent recognition system for locating areas prone to strong earthquakes in the Andean and Caucasian mountain belts. *Izv. Phys. Solid Earth* **2016**, *52*, 461–491. [CrossRef]
29. Vijay, R.K.; Nanda, S.J. Seismicity analysis using space-time density peak clustering method. *Pattern Anal. Appl.* **2020**, *24*, 181–201. [CrossRef]
30. Zaliapin, I.; Ben-Zion, Y. Earthquake clusters in southern California I: Identification and stability. *J. Geophys. Res. Solid Earth* **2013**, *118*, 2847–2864. [CrossRef]
31. Zaliapin, I.; Gabrielov, A.; Keilis-Borok, V.; Wong, H. Clustering Analysis of Seismicity and Aftershock Identification. *Phys. Rev. Lett.* **2008**, *101*, 018501. [CrossRef]
32. Telesca, L.; Golay, J.; Kanevski, M. Morisita-based space-clustering analysis of Swiss seismicity. *Phys. A Stat. Mech. Its Appl.* **2015**, *419*, 40–47. [CrossRef]
33. Rehman, K.; Burton, P.W.; Weatherill, G.A. K-means cluster analysis and seismicity partitioning for Pakistan. *J. Seismol.* **2013**, *18*, 401–419. [CrossRef]
34. Peresan, A.; Gentili, S. Identification and characterization of earthquake clusters: A comparative analysis for selected sequences in Italy and adjacent regions. *Boll. Geofis. Teor. Ed Appl.* **2020**, *61*, 57–80.
35. Melnikova, V.; Seredkina, A.; Gileva, N. Spatio-Temporal Patterns of the Development of Strong Seismic Activations (1999–2007) in the Northern Baikal Area. *Russ. Geol. Geophys.* **2020**, *61*, 96–109. [CrossRef]
36. Shang, X.; Li, X.; Morales-Esteban, A.; Asencio-Cortés, G.; Wang, Z. Data Field-Based K-Means Clustering for Spatio-Temporal Seismicity Analysis and Hazard Assessment. *Remote Sens.* **2018**, *10*, 461. [CrossRef]
37. Telesca, L.; Alcaz, V.; Burtiev, R.; Sandu, I. Time-clustering analysis of the 1978–2008 sub-crustal seismicity of Vrancea region. *Nat. Hazards Earth Syst. Sci.* **2011**, *11*, 2335–2340. [CrossRef]
38. Aslam, B.; Naseer, F. A statistical analysis of the spatial existence of earthquakes in Balochistan: Clusters of seismicity. *Environ. Earth Sci.* **2020**, *79*. [CrossRef]
39. Matoza, R.S.; Shearer, P.M.; Lin, G.; Wolfe, C.J.; Okubo, P.G. Systematic relocation of seismicity on Hawaii Island from 1992 to 2009 using waveform cross correlation and cluster analysis. *J. Geophys. Res. Solid Earth* **2013**, *118*, 2275–2288. [CrossRef]
40. Al-Ahmadi, K.; Al-Amri, A.; See, L. A spatial statistical analysis of the occurrence of earthquakes along the Red Sea floor spreading: Clusters of seismicity. *Arab. J. Geosci.* **2013**, *7*, 2893–2904. [CrossRef]
41. Gvishiani, A.D.; Vorobieva, I.A.; Shebalin, P.N.; Dzeboev, B.A.; Dzeranov, B.V.; Skorkina, A.A. Integrated Earthquake Catalog of the Eastern Sector of the Russian Arctic. *Appl. Sci.* **2022**, *12*, 5010. [CrossRef]
42. Agayan, S.M.; Bogoutdinov, S.R.; Krasnoperov, R.I. Short introduction into DMA. *Russ. J. Earth Sci.* **2018**, *18*, 1–10. [CrossRef]
43. Agayan, S.M.; Bogoutdinov, S.R.; Dobrovolsky, M.N. Discrete Perfect Sets and Their Application in Cluster Analysis. *Cybern. Syst. Anal.* **2014**, *50*, 176–190. [CrossRef]

44. Bogoutdinov, S.R.; Odintsova, A.A.; Pirogova, A.S. Search for extremity zones with discrete mathematical analysis algorithms to identify risks when drilling based on geophysical data. *Russ. J. Earth Sci.* **2022**, *22*, 1–9. [CrossRef]
45. Agayan, S.; Bogoutdinov, S.; Kamaev, D.; Kaftan, V.; Osipov, M.; Tatarinov, V. Theoretical Framework for Determination of Linear Structures in Multidimensional Geodynamic Data Arrays. *Appl. Sci.* **2021**, *11*, 11606. [CrossRef]
46. Agayan, S.M.; Bogoutdinov, S.R.; Dzeboev, B.A.; Dzeranov, B.V.; Kamaev, D.A.; Osipov, M.O. DPS Clustering: New Results. *Appl. Sci.* **2022**, *12*, 9335. [CrossRef]
47. Agayan, S.M.; Tatarinov, V.N.; Gvishiani, A.D.; Bogoutdinov, S.R.; Belov, I.O. FDPS algorithm in stability assessment of the Earth's crust structural tectonic blocks. *Russ. J. Earth Sci.* **2020**, *20*, 1–14. [CrossRef]
48. Agayan, S.M.; Losev, I.V.; Belov, I.O.; Tatarinov, V.N.; Manevich, A.I.; Pasishnichenko, M.A. Dynamic Activity Index for Feature Engineering of Geodynamic Data for Safe Underground Isolation of High-Level Radioactive Waste. *Appl. Sci.* **2022**, *12*, 2010. [CrossRef]
49. Agayan, S.; Bogoutdinov, S.; Soloviev, A.; Sidorov, R. The Study of Time Series Using the DMA Methods and Geophysical Applications. *Data Sci. J.* **2016**, *15*. [CrossRef]
50. Dzeboev, B.A.; Karapetyan, J.K.; Aronov, G.A.; Dzeranov, B.V.; Kudin, D.V.; Karapetyan, R.K.; Vavilin, E.V. FCAZ-recognition based on declustered earthquake catalogs. *Russ. J. Earth Sci.* **2020**, *20*, 1–9. [CrossRef]
51. Işık, E.; Harirchian, E. A Comparative Probabilistic Seismic Hazard Analysis for Eastern Turkey (Bitlis) Based on Updated Hazard Map and Its Effect on Regular RC Structures. *Buildings* **2022**, *12*, 1573. [CrossRef]
52. Işık, E.; Harirchian, E.; Büyüksaraç, A.; Ekinci, Y.L. Seismic and Structural Analyses of the Eastern Anatolian Region (Turkey) Using Different Probabilities of Exceedance. *Appl. Syst. Innov.* **2021**, *4*, 89. [CrossRef]
53. Buyuksarac, A.; Isik, E.; Harirchian, E. A case study for determination of seismic risk priorities in Van (Eastern Turkey). *Earthq. Struct.* **2021**, *20*, 445–455. [CrossRef]
54. Bülbül, M.A.; Harirchian, E.; Işık, M.F.; Aghakouchaki Hosseini, S.E.; Işık, E. A Hybrid ANN-GA Model for an Automated Rapid Vulnerability Assessment of Existing RC Buildings. *Appl. Sci.* **2022**, *12*, 5138. [CrossRef]
55. Gupta, I. Probabilistic seismic hazard analysis method for mapping of spectral amplitudes and other design specific quantities to estimate the earthquake effects on manmade structures. *ISET J. Earthq. Technol.* **2007**, *44*, 127–167.
56. Robinson, T.R. Scenario ensemble modelling of possible future earthquake impacts in Bhutan. *Nat. Hazards* **2020**, *103*, 3457–3478. [CrossRef]
57. Tehseen, R.; Farooq, M.S.; Abid, A. Earthquake Prediction Using Expert Systems: A Systematic Mapping Study. *Sustainability* **2020**, *12*, 2420. [CrossRef]
58. Gvishiani, A.D.; Agayan, S.M.; Losev, I.V.; Tatarinov, V.N. Geodynamic hazard assessment of a structural block holding an underground radioactive waste disposal facility. *Min. Inform. Anal. Bull.* **2021**, 5–18. [CrossRef]
59. Ester, M.; Kriegel, H.P.; Sander, J.; Xu, X. A density-based algorithm for discovering clusters in large spatial databases with noise. In Proceedings of the Second International Conference on Knowledge Discovery and Data Mining (KDD-96), Portland, OR, USA, 2–4 August 1996; AAAI Press: Washington, DC, USA, 1996; pp. 26–231.
60. Ankerst, M.; Breunig, M.; Kriegel, H.P.; Sander, J. OPTICS: Ordering Points To Identify the Clustering Structure. In Proceedings of the ACM SIGMOD International Conference on Management of Data, Philadelphia, PA, USA, 31 May–3 June 1999; ACM Press: New York, NY, USA, 1999; pp. 49–60.
61. Bondur, V.; Gokhberg, M.; Garagash, I.; Alekseev, D. Features of the modelled stress-strain state dynamics prior to the M7.1 2019 Ridgecrest earthquake in Southern California. *Russ. J. Earth Sci.* **2022**, 1–19. [CrossRef]

Disclaimer/Publisher's Note: The statements, opinions and data contained in all publications are solely those of the individual author(s) and contributor(s) and not of MDPI and/or the editor(s). MDPI and/or the editor(s) disclaim responsibility for any injury to people or property resulting from any ideas, methods, instructions or products referred to in the content.